The Effective 3D MRI Reconstruction Method Driven by the Fusion Strategy in NSST Domain

Jin Huang[1], Lei Wang[2]*, Muhammad Tahir[3], Tianqi Cheng[4], Xinping Guo[5], Yuwei Wang[6], ChunXiang Liu[7]*
School of Computer Science and Technology, Shandong University of Technology, Zibo, 255000, China[1,2,4,5,6]
Department of Computer Science, Mohammad Ali Jinnah University, Block 6 PECHS, Karachi, 75400, Pakistan[3]
School of Resources and Environmental Engineering, Shandong University of Technology, Zibo, 255000, China[7]

***Abstract*—The 3D reconstruction of medical images plays an important role in modern clinical diagnosis. Although the analytic-based, the iterative-based and the deep learning-based methods have been popularly used, there are still many problems to deal with. The analysis-based methods are not accurate enough, the iteration-based methods are computationally intensive, and the deep learning based methods are heavily dependent on the training of the data. To solve the default that only the single scan sequence is included in the traditional methods, a reconstruction method driven by the non-subsampled shearlet transform (NSST) and the algebraic reconstruction technique (ART) is proposed. Firstly, the multiple magnetic resonance imaging (MRI) sequences are decomposed into high-frequency and low-frequency components by NSST. Secondly, the low-frequency parts are fused with the weighted average fusion scheme and the high-frequency parts are fused with the weighted coefficient scheme that guided by the regional average gradient and energy. Finally, the 3D reconstruction is performed by using the ART algorithm. Compared with the traditional reconstruction methods, the proposed method is able to capture more information from the multiple MRI sequences, which makes the reconstruction results much clearer and more accurate. By comparing with the single-sequence reconstruction model without fusion, the experiments fully prove the accuracy and effectiveness.**

Keywords*—Multiple magnetic resonance imaging; 3D reconstruction; non-subsampled shearlet transform; the algebraic reconstruction

I. INTRODUCTION

Nowadays, the modern imaging technologies, such as the nuclear magnetic resonance imaging (MRI), the computer tomography (CT), sonography, have been popularly used by the clinicians to obtain the two-dimensional tomographic images of patients. These diagnostic techniques have great advantages over the traditional diagnostic methods in observing the structure of human tissue, extracting relevant information, and determining a reasonable course of treatment [1]. For example, CT can help to determine the size, shape, and extent of lesions in the examination of lung cancer and show the clear structure of the bone [2-3]. Ultrasound detection can be used to screen the fetus for malformations during the pregnancy check-up [4-5], and MRI can accurately show the tissue and tumors in the brain without interference from the skull during cranial examinations [6-7].

However, 2D images are isolated, static and abstract, making it difficult for physicians to infer the shape, size and location of the lesions. Thus, it is necessary to convert 2D images into relational, dynamic, and concrete 3D reconstruction models [8-10]. On the other hand, the 3D reconstruction has been successfully applied in recent years, all of which can be classified into three schemes: the analytic scheme, the iterative scheme and deep learning scheme. For the first one, Feldkamp et al. proposed the filtered back-projection (FBP) [11-12], it solves the shape artifacts by convolving the projection before back-projection under each acquisition projection. FBP is very fast and supports the targeted reconstruction. But the filters are easily to produce s obvious vibration and blur in the results. For the second scheme, Gordan et al. proposed the algebraic reconstruction technique (ART), which the reconstruction procedure is treated to be the problem of solving the mathematic equations [13-14]. It calculates the value of each voxel by solving the linear equations. In addition, the loop iterations will continuously optimize the objective function until the error is small enough to determine the simulated projection data is fully matched with the detection data. For the third scheme, Wang S et al. proposed the famous DeepVO model [15], where the recurrent convolutional neural network is employed to infer the pose directly from the source videos without any traditional visual odometry, improving the visual odometry loop in 3D reconstruction [16]. It can meet the real-time performance very well, but the accuracy is not satisfactory. Panigrahy C et al. proposed an improved PCNN model which uses the adaptive dual channel with a weighted parameter to fuse MRI sequences and SPECT images, and Seal A et al. proposed a wavelet transform method with random forest and à-trous strategy to fuse PET and CT images [17-18]. They fused different types of images, combining information from different images into one image, and have achieved very good results of reconstruction.

Considering the advantages and limitations of all these methods, with the aim of solving the problem that only one sequence can be included in the reconstruction, a pre-fused 3D reconstruction method is proposed. Firstly, multiple MRI sequences were decomposed into high-frequency and low-frequency parts, and then different strategies are used to fuse the low-frequency and high-frequency parts. Finally, ART reconstruction is performed on the images after fusion. This method concentrates the useful information of multiple sequences into one reconstruction model, which is helpful to observe the overall morphology of the lesions and their relationship with the surrounding structures in multiple directions and angles [19-20].

The contributions in this paper are summarized as follows: (1) The NSST transform based fusion algorithm is used to fuse the multiple MRI sequences and collect the useful information of each sequence; (2) The ART algorithm is used for 3D reconstruction, which makes the reconstruction be more accurate; (3) The Multiple sequences are pooled into a reconstruction model, which is more informative than the reconstruction model of a single sequence.

The rest of the paper is organized as follows. Section II briefly describes the related work and Section III, the proposed model. In Section IV, extensive experiments are used to evaluate the model. Finally, Section V gives a few concluding remarks.

II. Related Work

A. The Nuclear Magnetic Resonance Imaging Sequences

In order to evaluate the various parameters of the detected tissue, weighted scans that highlight certain tissue characteristics can be obtained by adjusting the time parameters. Short echo time and repetition time can generate T1 sequence, long echo time and repetition time can generate T2 sequence and T1CE sequence can be generated by injecting contrast agent into the blood before MRI [21-22].

In Fig. 1, the differences between the three sequences are shown. In the T1-weighted image, the white is white matter, the gray is gray substance, and the black is cerebrospinal fluid, so the T1-weighted scans can be used for tomographic anatomy [23]. In the T2-weighted image, the highlighted area is usually the lesion, so the location and size of the lesion can be clearly shown from the T2-weighted scans [24]. As in T2-weighted image, the highlighted area in T1CE-weighted image is generally the lesion [25]. Furthermore, because of the contrast agent, it can be used to reveal the intra-tumor conditions and discriminate the tumor and non-tumor lesions.

B. The Detail of the Non-Subsampled Shearlet Transform

The NSST is an advanced multi-scaled geometric analysis tool with translation invariance, simple computational cost and multi-dimension, which has been popularly used in many fields of computer vision [26-27].

As shown in Fig. 2, the process mainly includes two parts: non-subsampled pyramid (NSP) decomposition and direction localization [28]. The NSP uses a two-channel non-down-sampling filter bank to make the multi-scale [29]. The input image is decomposed by one level of NSP to produce a low-frequency part and a high-frequency part, and each subsequent level of NSP is iterated over the low-pass component to obtain the singularities in the image. So that, the two-dimensional image is decomposed by levels of NSP to obtain the subband images with the same size of the input image, which includes one low-frequency image and images of the same size but different scales. The direction localization is implemented by a shearlet filter (SF). From the pseudo-polarized coordinates to Cartesian coordinates, the Meyer wavelet is applied to construct a window function to obtain the shearlet filter, and the decomposed sub-band image is convolved with the Meyer window function in two dimensions to obtain the directional subband image.

Another good property is that there is no down-sampling operation in the process of the NSST, which makes it have translation invariance [30]. In addition, the NSST has very good localization properties and high directional sensitivity, and satisfies the parabolic scaling properties. All the above properties guarantee the great ability of capturing the important medical features from the MRI.

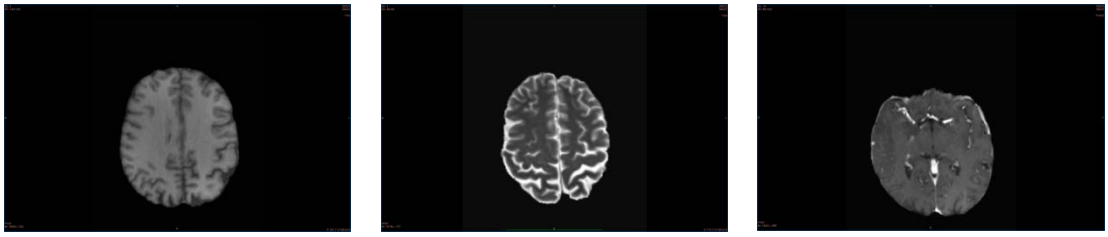

(a) T1 (b) T2 (c) T1CE

Fig. 1. Three examples of the MRI.

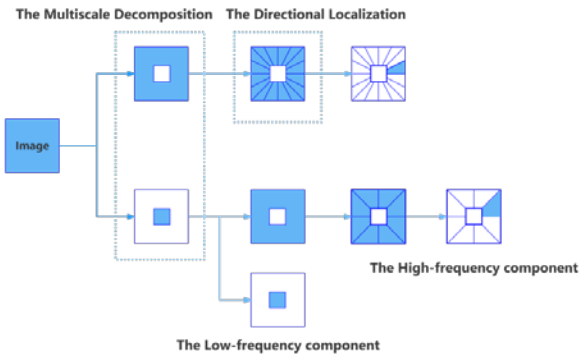

Fig. 2. The discrete process of the NSST.

C. The Algebraic Reconstruction

The basic idea of the Algebraic Reconstruction Technique (ART) is to transform the image reconstruction problem into a problem of solving a linear system of equations [31-32]. As the 2D section of a 3D object shown in the Fig. 3, it is divided into several discrete pixel regions, and set the image values inside each pixel region to be uniformly distributed, and denote the image values in the i-th pixel region by X_i.

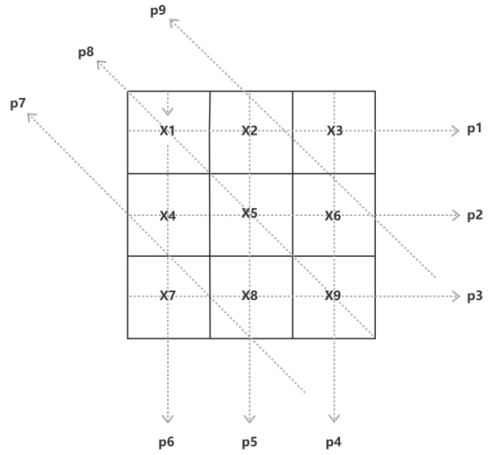

Fig. 3. The detection process to the 2D section.

Similarly, the detector plane is divided into the discrete projection cells and denote the projection value in the j projection cell by pj . Then the detection process can be represented by a linear system as Equation (1).

$$\begin{pmatrix} x_{11} & x_{21} & \cdots & x_{m1} \\ x_{12} & x_{22} & \cdots & x_{m2} \\ \cdots & \cdots & \cdots & \cdots \\ x_{1n} & x_{2n} & \cdots & x_{mn} \end{pmatrix} \begin{pmatrix} f_1 \\ f_2 \\ \cdots \\ f_n \end{pmatrix} = \begin{pmatrix} p_1 \\ p_2 \\ \cdots \\ p_n \end{pmatrix} \quad (1)$$

In theory, tomographic images can be obtained by solving the algebraic equations. But in practice this approach cannot be ideally achieved. Firstly, the system of equations has a unique solution only when the projection data is equal to the unknown image pixels, which is not actually satisfied. Secondly, there is seriously statistical noise in the projection data P obtained by nuclear medicine imaging, so when the ill-conditioned nature of the system transmission matrix C is serious, the direct solution method will be seriously disturbed by noise, and the obtained solution may be the same as the real situation. Therefore, an iterative method is usually used [33].

D. The Limitations of the Previous Research

In general, the 3D reconstruction methods can be classified into three types: the analytic-based methods, the iterative-based methods and the deep learning-based methods. The analytic-based methods are often only applicable to a certain scenario. They have achieved great performance, but there still have some problems. The iterative-based methods optimize the reconstruction process by using the idea of algebraic iteration, they require extensive calculations. The deep learning-based methods usually employee the complex neural networks, which require large amounts of data to train.

III. Proposed Method

A. The Whole Process

The whole process of the algorithm is shown in the Fig.4: (1) Perform the NSST decomposition on the three groups of MRI sequences to obtain their respective high and low frequency components; (2) For the low frequency part, the weighted fusion method driven by guided filtering is used [34]; for the high frequency part, the fusion rule combining the average gradient, the regional energy index weighting coefficient and the larger absolute value is used [35]; (3) Perform ART on the fused information to obtain a 3D reconstruction model.

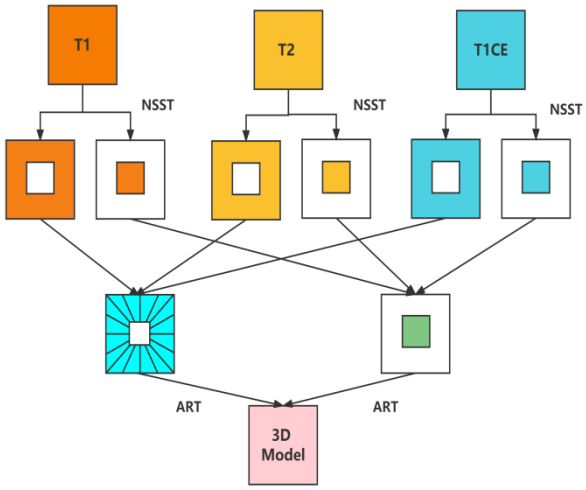

Fig. 4. The whole process of the proposed reconstruction method.

B. The Extraction and Fusion of the Information

The low-frequency part contains the energy of the image, and the coarse features in the image is correlated. Each pixel is not independent, and the pixels at any position of the pixel can show strong correlation. The low-frequency part is simply taken the maximum value or weighted average. Therefore, the weighted fusion method driven by the guided filtering is applied in this part. Taking the selected slices in the sequence as the guiding image and the other slices as the input image, use the low-frequency components of the original slices to subtract the respective output images of the guided filter to obtain the sharpened image. The improved regional sum of Laplacian energy (SML) of the sharpened image is used to determine the fusion weights, and then the low-frequency subband coefficients of the fused image are calculated by Equation (2). The A and B in Equation (2) can be expressed by Equation (3) and Equation (4).

$$A(m,n) = \frac{A}{B} \quad (2)$$

$$A = \sum_{i=1}^{3} \omega t_i(m,n) a_i(m,n) \quad (3)$$

$$B = \sum_{i=1}^{3} \omega t_i(m,n) \quad (4)$$

The high-frequency parts are mainly the feature information, such as the edge, textures of the input image. The human visual system is not sensitive to pixels, but sensitive to the edge, orientation and texture information of the image. The regional energy retains the input image details and also reflects the correlation of the input image. The larger the area energy,

the richer is the detailed information of the image. The average gradient of the image reflects the sharpness of the image, as well as the expressive ability of the image to the contrast of small details and the texture transformation characteristics of the image. Therefore, this paper proposes a fusion rule of regional average gradient and regional energy to jointly guide the weighting coefficient for high-frequency components. The following rules are adopted for high frequency components as Equation (5).

$$T^{l,k}(i,j)=\frac{1}{m\times n}\sum_{i=0}^{m-1}\sum_{i=0}^{n-1}\sqrt{\frac{A}{2}} \tag{5}$$

In Equation (5), A can be expressed as Equation (6).

$$A=(\frac{\partial f(i,j)}{\partial x})^2+(\frac{\partial f(i,j)}{\partial y})^2 \tag{6}$$

In Equation (3), m and n are the rows and columns of the sequence slice. Respectively, $f(i,j)$ is the coefficient of the high-frequency component at pixel point (i,j), and $T^{l,k}(i,j)$ is the average gradient at pixel (i,j).

C. The Reconstruction Algorithm

It is well known that the reconstruction can be transformed into a system of linear equations as Equation (7).

$$\begin{cases} c_1 f = p_1 \\ c_2 f = p_2 \\ .... \\ c_n f = p_n \end{cases} \tag{7}$$

$c_j=(c_{1j},c_{2j},c_{3j}\cdots c_{Nj})$ is the vector dot product operation. If we take the N components of the image to form an N dimensional space, then each set of estimates of the image is a point in this N dimensional space, and each of the linear equations in the set of equation is an $N-1$ dimensional hyperplane in this N dimensional space, which is orthogonal to the vector c_j. If the system of linear equations has a unique solution, then these N hyperplanes have a unique intersection which is the solution we require.

From the initial image estimate f^0, project this point onto the hyperplane represented by the first equation, use the projection point as the first image estimate f^1, project the projection point onto the second hyperplane again to obtain a new projection point f^2, continue to implement this procedure until the projection of all equations is carried out. Then the process of f^n can be expressed by the Equation (8).

$$f^n=f^{n-1}-\frac{(f^{n-1}\bullet c_n-p_n)}{c_n} \tag{8}$$

Finally, it can be further deduced into the Equation (9).

$$f^n=f_i^{n-1}-c_{in}\frac{\sum_i(f_i^{n-1}c_{in})}{\sum_i c_{in}^2} \tag{9}$$

IV. Experiments and Discussion

The platform used for the experiments is the CentOS Linux x64, with CPU of Intel(R) Xeon(R) Silver 4114 and GPU of NVIDIA Tesla GPU in the memory of 16GB.

To verify the effectiveness of the fusion method and the effect of the 3D reconstruction result, two experiments with two datasets are implemented. Firstly, to verify the fusion method, the T1, T2, T1CE sequences are compared with the fused sequences. The image definition (FD), standard deviation (STD), edge strength (EIN), information entropy (EN), and spatial frequency (SF) are the objective evaluation criterion for the effect of the fusion method. EN, STD and SF are the typical metrics of image fusion. EIN and FD can measure the segmentation and sharpness of the image edges, the clearer the edges; the more complete the shape of the individual organs will be after 3D reconstruction [36].

As shown in Table I, all the five metrics of the fused sequence are higher than the original sequence, proving the effectiveness of the proposed fusion method.

TABLE I. The comparison of T1, T2, T1CE and the fusion results

Methods	*EN*	*STD*	*SF*	*EIN*	*FD*
T1	2.64	38.35	6.68	162.21	105.47
T2	2.55	35.42	6.74	164.14	107.31
T1CE	2.56	40.94	7.17	165.45	108.95
Fusion	2.72	40.97	7.22	165.56	110.63

The ART is used to model the original sequences and the fused sequence separately, and observe the details of the model from the top, bottom, left and right directions to compare the texture, structure and clarity of the model.

As shown in Fig. 5 to Fig. 6, the images in (a)-(d) are 3D reconstructions of T1 sequence, (e)-(h) are 3D reconstructions of T2 sequence, (i)-(l) are 3D reconstructions of T1CE sequence and (m)-(p) are 3D reconstructions of fused sequence. The pictures of the top left, right and bottom directions are cropped. The bottom right corner is an enlarged image of the same region, so the details of the reconstructed model can be clearly compared. In the first three sets of reconstruction models, some areas are blurred and not smooth enough, but in

the proposed reconstruction model, the same areas are more smooth and clear without blurring. By comparing the enlarged area, the proposed reconstruction model is also clearly visible after zooming it, unlike the unfused reconstruction model that has blurring. The fused reconstruction model has clear texture, rich detailed information and good visual effect. In the comparison of the reconstruction model and the reconstruction model before fusion, especially in the enlarged areas, it can be found that the results from the reconstruction method after fusion is much smooth, more feature details are remained, and the visual quantity is much better than the other results. All the facts fully prove the effectiveness and progressiveness of the proposed model.

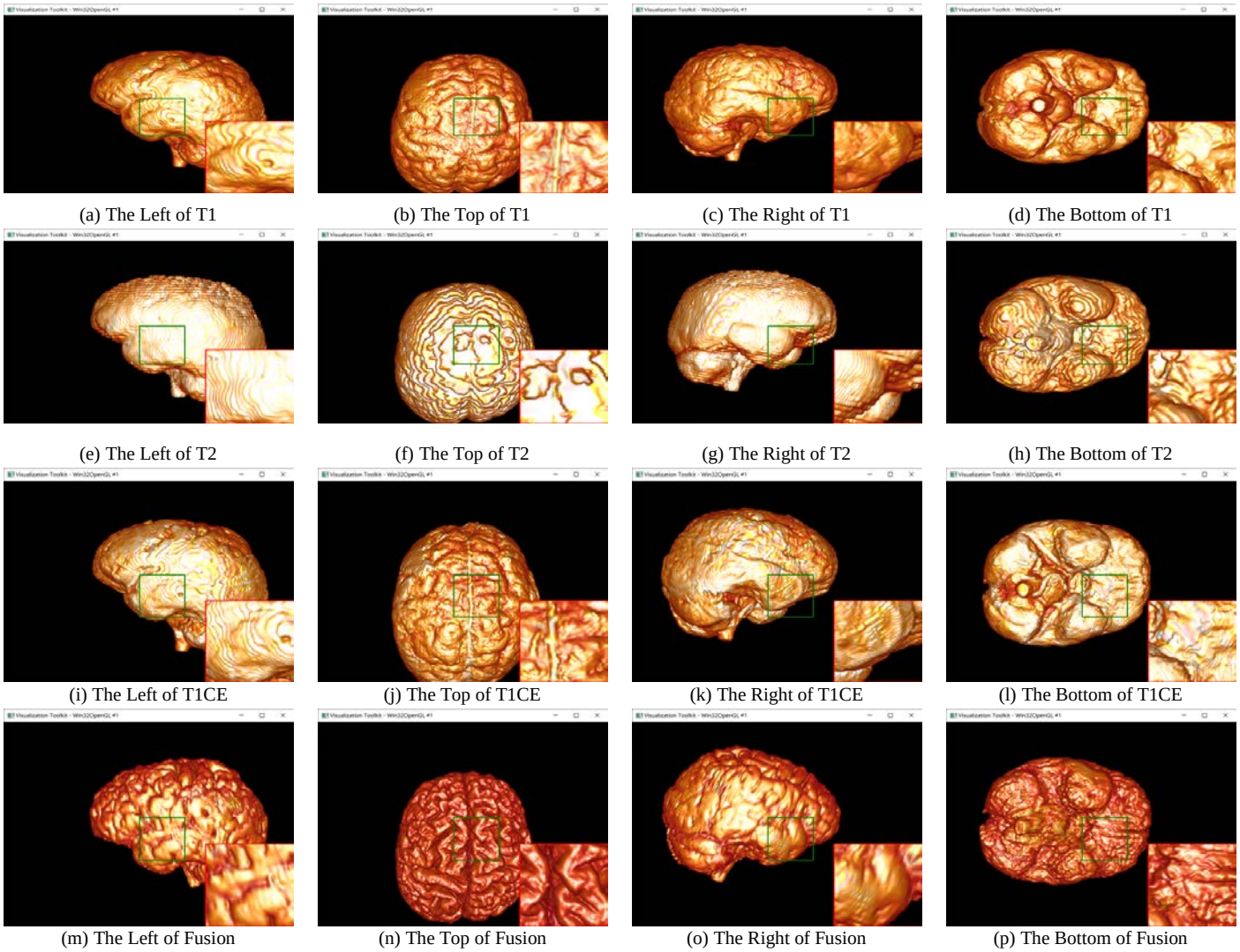

(a) The Left of T1 (b) The Top of T1 (c) The Right of T1 (d) The Bottom of T1

(e) The Left of T2 (f) The Top of T2 (g) The Right of T2 (h) The Bottom of T2

(i) The Left of T1CE (j) The Top of T1CE (k) The Right of T1CE (l) The Bottom of T1CE

(m) The Left of Fusion (n) The Top of Fusion (o) The Right of Fusion (p) The Bottom of Fusion

Fig. 5. The comparison of the 3D reconstruction results for the first group.

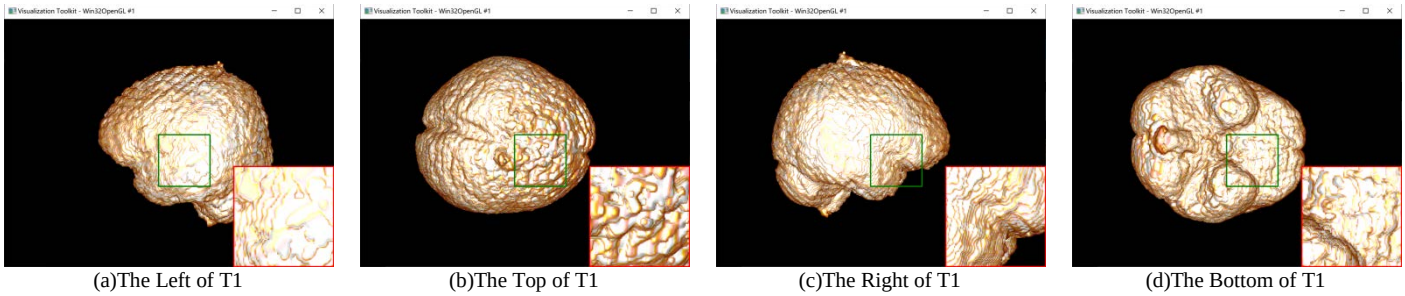

(a)The Left of T1 (b)The Top of T1 (c)The Right of T1 (d)The Bottom of T1

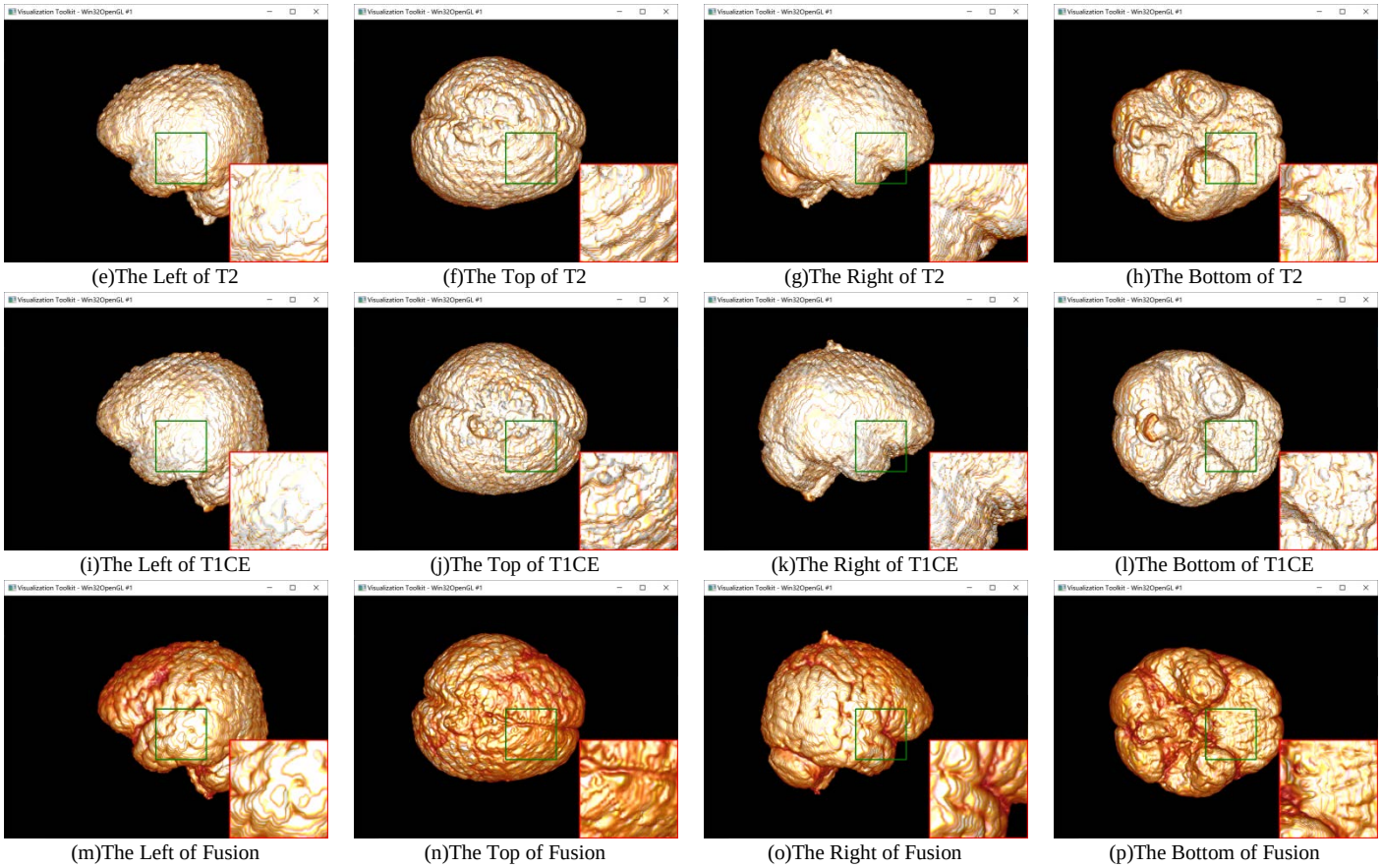

(e)The Left of T2 (f)The Top of T2 (g)The Right of T2 (h)The Bottom of T2

(i)The Left of T1CE (j)The Top of T1CE (k)The Right of T1CE (l)The Bottom of T1CE

(m)The Left of Fusion (n)The Top of Fusion (o)The Right of Fusion (p)The Bottom of Fusion

Fig. 6. The comparison of 3D reconstruction results for the second group.

V. Conclusion

An effective 3D reconstruction method, driven by NSST fusion scheme and ART, is proposed in this paper. Compared with other reconstruction methods, the reconstructed model can maintain more feature information by fusing multiple MRI sequences before reconstruction, which successfully meets the need that the reconstructed model contains more MRI sequence information. The post-fusion reconstructed model is compared with the pre-fusion reconstructed model by careful experiments. The proposed reconstructed model after fusion produces the good results with much clearer texture, smoother surface, and more detailed feature information.

In the future work, the proposed model will be optimized and extended to the other tasks of reconstruction, such as the Positron Emission Tomography (PET) and the Single-Photon Emission Computed Tomography (SPECT).

Acknowledgment

This study was supported by: A project ZR2021MF017 supported by Shandong Provincial Natural Science Foundation; The National Natural Science Foundation of China (61502282); A project ZR2020MF147 supported by Shandong Provincial Natural Science Foundation; The SDUT & Zibo City Integration Development Project(2020SNPT0055).

References

[1] Abadi E, Segars W P, Tsui B M W, et al. Virtual clinical trials in medical imaging: a review[J]. Journal of Medical Imaging, 2020, 7(4): 042805.

[2] Kennedy K, Hulbert A, Pasquinelli M, et al. Impact of CT screening in lung cancer: Scientific evidence and literature review[C]//Seminars in Oncology. WB Saunders, 2022.

[3] Zhang G, Jiang S, Yang Z, et al. Automatic nodule detection for lung cancer in CT images: A review[J]. Computers in biology and medicine, 2018, 103: 287-300.

[4] Shainker S A, Coleman B, Timor-Tritsch I E, et al. Special Report of the Society for Maternal-Fetal Medicine Placenta Accreta Spectrum Ultrasound Marker Task Force: Consensus on definition of markers and approach to the ultrasound examination in pregnancies at risk for placenta accreta spectrum[J]. American Journal of Obstetrics and Gynecology, 2021, 224(1): B2-B14.

[5] Leung Y, Shim H H, Wilkens R, et al. The role of bowel ultrasound in detecting subclinical inflammation in pregnant women with Crohn's disease[J]. Journal of the Canadian Association of Gastroenterology, 2019, 2(4): 153-160.

[6] Wadhwa A, Bhardwaj A, Verma V S. A review on brain tumor segmentation of MRI images[J]. Magnetic resonance imaging, 2019, 61: 247-259.

[7] Abd-Ellah M K, Awad A I, Khalaf A A M, et al. A review on brain tumor diagnosis from MRI images: Practical implications, key achievements, and lessons learned[J]. Magnetic resonance imaging, 2019, 61: 300-318.

[8] Pichat J, Iglesias J E, Yousry T, et al. A survey of methods for 3D histology reconstruction[J]. Medical image analysis, 2018, 46: 73-105.

[9] Singh S P, Wang L, Gupta S, et al. 3D deep learning on medical images: a review[J]. Sensors, 2020, 20(18): 5097.

[10] Ahishakiye E, Bastiaan Van Gijzen M, Tumwiine J, et al. A survey on deep learning in medical image reconstruction[J]. Intelligent Medicine, 2021, 1(03): 118-127.

[11] Yan Q, Dong H, Su J, et al. A review of 3D printing technology for medical applications[J]. Engineering, 2018, 4(5): 729-742.

[12] Shi L, Liu B, Yu H, et al. Review of CT image reconstruction open source toolkits[J]. Journal of X-ray Science and Technology, 2020, 28(4): 619-639.

[13] Greffier J, Frandon J, Larbi A, et al. CT iterative reconstruction algorithms: a task-based image quality assessment[J]. European radiology, 2020, 30(1): 487-500.

[14] Shen R H, He Y T, Ming W Q, et al. Electron tomography for sintered ceramic materials by a neural network algebraic reconstruction technique[J]. Journal of Materials Science & Technology, 2022, 100: 75-81.

[15] Wang S, Clark R, Wen H, et al. Deepvo: Towards end-to-end visual odometry with deep recurrent convolutional neural networks[C]//2017 IEEE international conference on robotics and automation (ICRA). IEEE, 2017: 2043-2050.

[16] Girshick R. Fast r-cnn[C]//Proceedings of the IEEE international conference on computer vision. 2015: 1440-1448.

[17] Han J, Cao Y, Xu L, et al. 3D Reconstruction Method based on Medical Image Feature Point Matching[J]. Computational and Mathematical Methods in Medicine, 2022, 2022.

[18] Maken P, Gupta A. 2D-to-3D: A Review for Computational 3D Image Reconstruction from X-ray Images[J]. Archives of Computational Methods in Engineering, 2022: 1-30.

[19] Panigrahy C, Seal A, Mahato N K. MRI and SPECT image fusion using a weighted parameter adaptive dual channel PCNN[J]. IEEE Signal Processing Letters, 2020, 27: 690-694.

[20] Seal A, Bhattacharjee D, Nasipuri M, et al. PET-CT image fusion using random forest and à-trous wavelet transform[J]. International journal for numerical methods in biomedical engineering, 2018, 34(3): e2933.

[21] Wolf M, de Boer A, Sharma K, et al. Magnetic resonance imaging T1- and T2-mapping to assess renal structure and function: a systematic review and statement paper[J]. Nephrology Dialysis Transplantation, 2018, 33(suppl_2): ii41-ii50.

[22] Baessler B, Luecke C, Lurz J, et al. Cardiac MRI texture analysis of T1 and T2 maps in patients with infarctlike acute myocarditis[J]. Radiology, 2018, 289(2): 357-365.

[23] Warnica W, Al-Arnawoot A, Stanimirovic A, et al. Clinical impact of cardiac MRI T1 and T2 parametric mapping in patients with suspected cardiomyopathy[J]. Radiology, 2022: 220067.

[24] Yue Z, Wang X, Wang Y, et al. Clinical-Radiomics Nomogram from T1W, T1CE, and T2FS MRI for Improving Diagnosis of Soft-Tissue Sarcoma[J]. Molecular Imaging and Biology, 2022: 1-12.

[25] Yue Z, Wang X, Wang Y, et al. Clinical-Radiomics Nomogram from T1W, T1CE, and T2FS MRI for Improving Diagnosis of Soft-Tissue Sarcoma[J]. Molecular Imaging and Biology, 2022: 1-12.

[26] Huang Y, Bi D, Wu D. Infrared and visible image fusion based on different constraints in the non-subsampled shearlet transform domain[J]. Sensors, 2018, 18(4): 1169.

[27] Tan W, Tiwari P, Pandey H M, et al. Multimodal medical image fusion algorithm in the era of big data[J]. Neural Computing and Applications, 2020: 1-21.

[28] Yin M, Liu X, Liu Y, et al. Medical image fusion with parameter-adaptive pulse coupled neural network in nonsubsampled shearlet transform domain[J]. IEEE Transactions on Instrumentation and Measurement, 2018, 68(1): 49-64.

[29] Radhakrishnan A, Uhler C, Belkin M. Downsampling leads to image memorization in convolutional autoencoders[J]. 2018.

[30] Jose J, Gautam N, Tiwari M, et al. An image quality enhancement scheme employing adolescent identity search algorithm in the NSST domain for multimodal medical image fusion[J]. Biomedical Signal Processing and Control, 2021, 66: 102480.

[31] Komarov D A, Samouilov A, Ahmad R, et al. Algebraic reconstruction of 3D spatial EPR images from high numbers of noisy projections: an improved image reconstruction technique for high resolution fast scan EPR imaging[J]. Journal of Magnetic Resonance, 2020, 319: 106812.

[32] Vaniqui A, Schyns L E J R, Almeida I P, et al. The effect of different image reconstruction techniques on pre-clinical quantitative imaging and dual-energy CT[J]. The British journal of radiology, 2019, 92(1095): 20180447.

[33] Komarov D A, Samouilov A, Ahmad R, et al. Algebraic reconstruction of 3D spatial EPR images from high numbers of noisy projections: an improved image reconstruction technique for high resolution fast scan EPR imaging[J]. Journal of Magnetic Resonance, 2020, 319: 106812.

[34] Shehanaz S, Daniel E, Guntur S R, et al. Optimum weighted multimodal medical image fusion using particle swarm optimization[J]. Optik, 2021, 231: 166413.

[35] Liu Y, Wang L, Cheng J, et al. Multi-focus image fusion: A survey of the state of the art[J]. Information Fusion, 2020, 64: 71-91.

[36] Kaur H, Koundal D, Kadyan V. Image fusion techniques: a survey[J]. Archives of computational methods in Engineering, 2021, 28(7): 4425-4447.